Clustering Strategy Based on Graph Method and Power Control for Frequency Resource Management in Femtocell and Macrocell Overlaid System

Hongjia Li, Xiaodong Xu, Dan Hu, Xiaofeng Tao, Ping Zhang, Song Ci, and Hui Tang

Abstract: **In order to control interference and improve spectrum efficiency in the femtocell and macrocell overlaid system (FMOS), we propose a joint frequency bandwidth dynamic division, clustering and power control algorithm (JFCPA) for orthogonal-frequency-division-multiple access-based downlink FMOS. The overall system bandwidth is divided into three bands, and the macro-cellular coverage is divided into two areas according to the intensity of the interference from the macro base station to the femtocells, which are dynamically determined by using the JFCPA. A cluster is taken as the unit for frequency reuse among femtocells. We map the problem of clustering to the MAX k-CUT problem with the aim of eliminating the inter-femtocell collision interference, which is solved by a graph-based heuristic algorithm. Frequency bandwidth sharing or splitting between the femtocell tier and the macrocell tier is determined by a step-migration-algorithm-based power control. Simulations conducted to demonstrate the effectiveness of our proposed algorithm showed the frequency-reuse probability of the FMOS reuse band above 97.6% and at least 70% of the frequency bandwidth available for the macrocell tier, which means that the co-tier and the cross-tier interference were effectively controlled. Thus, high spectrum efficiency was achieved. The simulation results also clarified that the planning of frequency resource allocation in FMOS should take into account both the spatial density of femtocells and the interference suffered by them. Statistical results from our simulations also provide guidelines for actual FMOS planning.**

Index Terms: **Clustering, femtocell, graph, interference management, power control, spectrum reuse.**

I. INTRODUCTION

Reduction of cell sizes and transmit distance are two of the most effective ways to improve system capacity and cellular coverage. These methods have resulted in a 1600-fold gain in system capacity improvement since 1957 [1]. As a result, significant interest is being focused on the femtocell, also known as home node B (HNB) and home enhanced node B (HeNB), which has been accepted by the third generation partnership project (3GPP) for standardization [2]. Hence, a new network architecture, comprising femtocell and macrocell tiers, was introduced. However, this new network architecture brings new challenges to the existing strategies of interference management and radio resource management (RRM), especially when femtocells are applied in densely populated countries or cities, such as China and New York.

First, due to spectral scarcity, femtocells and macrocells have to partially or totally share frequency bandwidth, which leads to the problem of cross-tier, co-channel interference between femtocells and macrocells. At the same time, in order to guarantee services to a large number of femtocells in the same macrocell coverage, femtocells need to fully reuse limited frequency resources, which results in the problem of co-tier, co-channel interference between femtocells.

Second, when compared with conventional hierarchical cellular systems (HCSs) [3], in which microcells are embedded in the macrocell, femtocell and macrocell overlaid systems (FMOSs) have their own unique features: the location and configuration of microcells are carefully planned in conventional HCSs, while femtocells are placed according to subscribers' requirements, which results in femtocells being randomly distributed; the coverage radius (10–50 m) of femtocells is one-tenth, or less, than that of microcells [4]. Therefore, RRM strategies for HCSs are not all suitable for FMOSs.

A. Related Work

Analyses of FMOS interference scenarios provide the bases for the design of interference management schemes. The femto forum [5] lists ten types of interference scenarios without covering any interference control methods. A qualitative analysis of FMOS interference scenarios is also provided [6].

A few studies have been conducted to address the problem of interference and RRM. These studies can be classified into two categories: The frequency partitioning scheme and the universal frequency reuse scheme.

In the frequency partitioning scheme, orthogonal frequency resources are allocated to the femtocell tier and the macrocell tier, respectively. Chandrasekhar *et al.* [7] proposed a strategy for determining the ratios of the frequency bandwidth allocated to the femtocell tier and the macrocell tier, which are bound to decrease spectrum efficiency. Based on the frequency partitioning scheme, Lee *et al.* [8] used the fractional frequency reuse (FFR) to mitigate inter-femtocell interference (i.e., co-tier in-

Manuscript received March 16, 2010; approved for publication by Seong-Lyun Kim, Division III Editor, August 28, 2011.

This work was supported by the National Science and Technology Special Project (No. 2009ZX03003-007-01), the NSFC Project (No. 61001116), the Key Project of Beijing Municipal Science & Technology Commission (No. D08080100620802), and the International Cooperation and Exchanges Project (No. S2010GR0902).

Part of this paper was presented at the 6th Int. Conf. on Wireless Communications, Networking and Mobile Computing, Chengdu, China, Sept. 2010.

H. Li, S. Ci, and H. Tang are with the High Performance Network Lab, Institute of Acoustics, Chinese Academy of Sciences, China, email: {lihj, sci, tangh}@hpnl.ac.cn.

X. Xu, D. Hu, X. Tao, and P. Zhang are with Key Laboratory of Universal Wireless Communication, Ministry of Education, Beijing University of Posts and Telecommunications, China, email: {xuxiaodong, vivianhudan, taoxf, pzhang}@bupt.edu.cn.

1229-2370/11/$10.00

terference) in multi-femtocell environments. Guvenc *et al.* [9] proposed a frequency assignment scheme for orthogonal frequency division multiple access (OFDMA) systems in which a femtocell-only frequency band is assigned to femtocells that are within a certain distance of the macro base station (mBS). However, inter-femtocell interference and frequency assignment among femtocells were not considered. Careful analysis of these work shows that cross-tier interference is eliminated at the cost of spectrum efficiency.

In the universal frequency reuse scheme, all frequency resources are available to both tiers. Chandrasekhar *et al.* [10] utilized a time-hopped code division multiple access (CDMA) scheme with universal frequency reuse in its uplink system capacity analysis, which is, in fact, equivalent to splitting the resource in the time domain instead of splitting it in the frequency domain. Thus, the loss of resource efficiency in an environment where radio resource is so scarce constitutes a major drawback. Lopez-Perez *et al.* [11] proposed a dynamic frequency planning (DFP) technique that regards femtocell users as macrocell users in order to operate conventional resource allocation—which is bound to decrease the macrocell system capacity as the number of femtocells increases. Jo *et al.* [12] proposed an open-loop and closed-loop power control scheme, in which femto mobile stations reduce their transmit power to mitigate their uplink interference to the mBS. Chu *et al.* [13] proposed a resource allocation scheme for the OFDMA downlink of two-tier femtocell networks in which every femtocell randomly selects only a subset of the available OFDMA resources for transmission. Careful analysis of these studies shows that although frequency resources are universally reused, the efficiency of other resources (e.g., time, power, etc.) is reduced in order to control the co-tier and cross-tier interference. In addition, interference control, spectrum efficiency improvement, power allocation, and inter-tier influence are not comprehensively considered.

From the above analyses, three main questions arise.

1) Is the frequency partitioning scheme or the universal frequency reuse scheme effective for the entire FMOS region?
2) Is there a hybrid frequency reuse scheme that comprehensively considers interference control, spectrum efficiency improvement, power allocation, and inter-tier influence, according to the characteristics of the FMOS scenario?
3) Can the hybrid scheme improve the spectrum efficiency and bring throughput gain?

B. Contribution

In an effort to solve the aforementioned problems, the following contributions are made in this paper.

1) An FMOS model is built and quantitative analysis provided from which the duality relationship of downlink and uplink interference scenarios is derived.
2) A hybrid scheme of frequency resource allocation on the basis of contribution 1) is proposed. The macrocell is divided into two areas: The interference sensitive area (ISA) and the not interference sensitive area (NISA). On the basis of the area divisions, the entire frequency bandwidth is divided into three bands: The FMOS reuse band, the femtocell dedicated band, and the macrocell dedicated band.
3) To achieve the area division and frequency bandwidth division described in contribution 2), the joint frequency bandwidth dynamic division, clustering and power control algorithm (JFCPA) is proposed in the OFDMA-based downlink FMOS.

The rest of this paper is organized as follows. Section II describes the system model and analyzes downlink and uplink interference scenarios of FMOS in detail. Section III depicts the the hybrid region and bandwidth division, and then presents the description, derivation and proof of the JFCPA. Section IV provides simulations and analyses for the JFCPA. Section V summarizes and concludes this paper.

II. SYSTEM MODEL AND ANALYSIS

A. FMOS Model and Assumptions

Consider a reference hexagonal macrocell with coverage radius R_M, which consists of the mBS, macro mobile stations (mMSs) and femtocells with disk coverage radius R_f, as depicted in Fig. 1. The set of mMSs in the macrocell is defined as S_M. Every femtocell consists of the femto BS (fBS) and femto mobile stations (fMSs). The set of femtocells is defined as S_F and the set of fMSs in femtocell i ($i \in S_F$) is defined as $S_{Fu,i}$. The transmit power of mBSs and fBSs with an omni-directional antenna are $P_{\mathrm{mBS}}^{\max}$ and $P_{\mathrm{fBS}}^{\max}$ respectively. According to [14], it is rational and practical that equal transmit power (denoted P_{mBS}) is imposed at mBS's subchannels, while adjustable transmit power is imposed at fBS's subchannels. Each fMS is allocated with only one subchannel, and the upper bound of transmit power per subchannel, denoted $P_{\mathrm{fBS}}^{s-\max}$, is calculated as $P_{\mathrm{fBS}}^{\max}$ divided by the maximum number of fMSs per femtocell. The allocated transmit power from fBS in the femtocell i ($i \in S_F$) to its serving fMS $\hat{i}$ ($\hat{i} \in S_{Fu,i}$) is denoted as $P_{\hat{i}}^{\mathrm{fBS}}$.

For convenient analysis, some assumptions need to be illustrated as follows.

Assumption 1: For analytical tractability, the co-channel interference from neighboring macrocells is ignored.

Assumption 2: When installing, provisioning, configuring or re-configuring an fBS, the geographical location of the fBS is obtainable by the operator [2]. Information on the location of femtocells is maintained in the femto gateway (GW) [2], which can be obtained by the following two methods.

1) When femtocell operators own both fixed and mobile networks (such as operators in China), because digital subscriber line (DSL) is used as the backhaul between femtocells and cellular networks, it is feasible to obtain the femtocell location via the position of the fixed network interface [15].
2) When femtocell operators do not have a fixed network, for example, Vodafone in the UK—which commercializes femtocells, but is not an internet provider—there are several ways to compute locations, which vary in cost and accuracy. For example, the location scheme in [16], which performs a weighted combination of the time difference of arrival (TDoA) and received signal strength (RSS) location schemes in femtocell environments, can also be used to obtain the location information without any additional equipment.

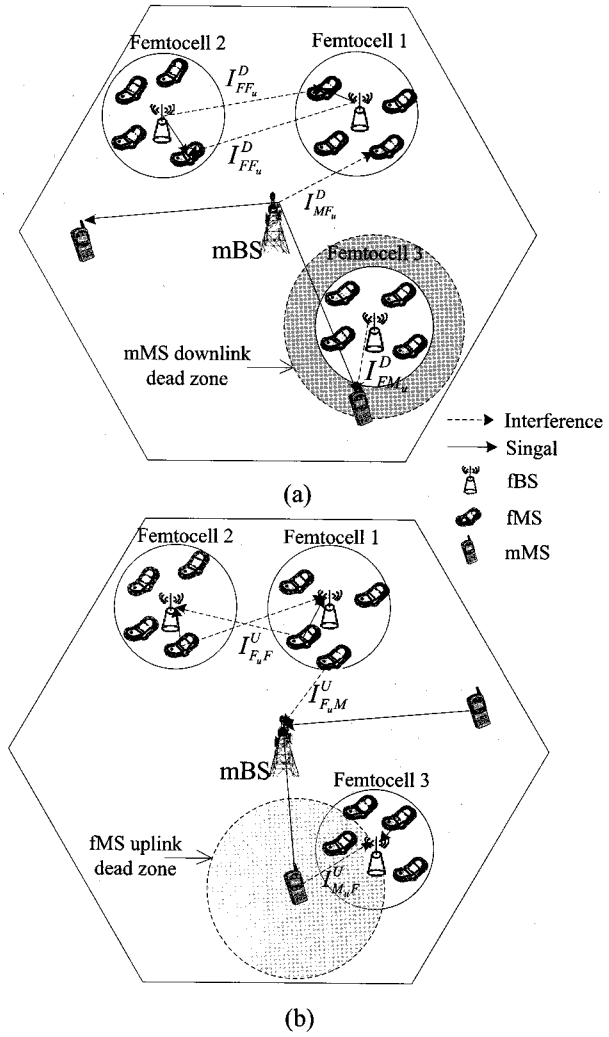

Fig. 1. Downlink and uplink interference scenarios in FMOS with universal frequency reuse: (a) Downlink interference scenario and (b) uplink interference scenario.

Assumption 3: The popular closed subscriber group configuration mode is adopted (CSG) [2]. In addition, the femtocell is the unit for QoS differentiation, which means that users belonging to the same femtocell have the same QoS class: For example, if a femtocell owner subscribes for 1 Mbps data rate service, the operator has to guarantee 1 Mbps service data rate for every fMS in the femtocell.

Assumption 4: There is an intermediate entity, called the femto GW, located between the fBSs and the mobile core network (CN). It acts as a "virtual" mBS for the CN and as a "virtual" CN entity for the fBSs. The interface between the fBSs and the femto GW can be S1 interface [17]. In one mBS coverage area, X2 interface exists between the "virtual" mBS (i.e., femto GW) and the mBS [17]. The femto GW can jointly optimize the radio parameters of the fBSs, for example, the transmit power and subchannel allocation. The femto GW can obtain all necessary knowledge related to the configuration of the femtocell system (e.g., path gains between BSs and MSs) through the X2 interface between the mBS and the femto GW, and S1 interface between the fBSs and the femto GW. In addition, information about the MS can be obtained by the BS via a feedback scheme [2].

Table 1. Downlink and uplink interference relationship.

Interference senario		Aggressor	Victim
Downlink	$I^D_{MF_u}$	mBS	fMS
	$I^D_{FF_u}$	fBS	Its non-camped fMS
	$I^D_{FM_u}$	fBS	Neighboring mMS
Uplink	$I^U_{F_MM}$	fMS	mBS
	$I^U_{F_MF}$	fMS	Its non-camped fBS
	$I^U_{M_uF}$	mMS	Neighboring fBS

B. Channel Propagation Model

The channel propagation model [10], [18] is represented as a combination of path-loss, penetration loss, and log-normal shadowing. The following four situations (identified by superscripts $m1, m2, f1$, and $f2$) are considered.

Outdoor link, i.e., mBS M to outdoor mMS k ($k \in S_M$),

$$G^{m1}_{Mk} = K_m |x_{Mk}|^{-\alpha} \chi_{Mk}. \tag{1}$$

Outdoor-to-indoor link, i.e., mBS M to indoor fMS $\hat{i}$,

$$G^{m2}_{M\hat{i}} = K_m |x_{M\hat{i}}|^{-\alpha} \chi_{M\hat{i}} WL^{-1}. \tag{2}$$

Indoor link, i.e., fBS in the femtocell i to its serving fMS $\hat{i}$ ($\hat{i} \in S_{Fu,i}$),

$$G^{f1}_{i\hat{i}} = K_f |x_{i\hat{i}}|^{-\beta} \chi_{i\hat{i}}. \tag{3}$$

Indoor-to-indoor link, i.e., fBS in the femtocell i to fMS $\hat{j}$ in the different femtocell j ($\hat{j} \in S_{Fu,j}, j \in S_F, j \neq i$),

$$G^{f2}_{i\hat{j}} = K_f |x_{i\hat{j}}|^{-\beta} \chi_{i\hat{j}} WL^{-2}. \tag{4}$$

In (1) to (4), α and β are the outdoor path-loss exponent (usually in the range $[3.5, 4.5]$) and the indoor path-loss exponent (usually in the range $[2.5, 3.5]$), respectively. $|x_{**}|$ is the distance between BS and MS. WL is the penetration loss. K_m and K_f, which are unitless constants depending on the wavelength of radio frequency (RF) carrier c/f_c and outdoor or indoor reference distance d_{om} or d_{of}, are defined as

$$K_m \triangleq d_{om}^{\alpha-2} [c/(4\pi f_c)]^2, \tag{5}$$

$$K_f \triangleq d_{of}^{\beta-2} [c/(4\pi f_c)]^2. \tag{6}$$

χ_{**} is the log-normal shadowing between BS and MS, and $10 \log \chi_{**} \sim N(0, \sigma^2)$.

C. Analysis of FMOS Downlink and Uplink Interference Scenarios

In the universal frequency reuse scenario, FMOS interference, shown in Figs. 1(a) and 1(b), can be grouped as shown in Table 1. First, three kinds of downlink interferences are quantitatively examined as follows.

1) $I^D_{MF_u}$ (mBS co-channel interference at fMS): mBS M interference at any fMS $\hat{i}$ ($\hat{i} \in S_{Fu,i}, i \in S_F$) is represented as $I^D_{MF_u} = P_{\mathrm{mBS}} K_m |x_{M\hat{i}}|^{-\alpha} \chi_{M\hat{i}} W L^{-1}$. The signal received by fMS $\hat{i}$ from its serving fBS i is $S^D_f = P^{\mathrm{fBS}}_{\hat{i}} K_f |x_{i\hat{i}}|^{-\beta} \chi_{i\hat{i}}$. When only considering $I^D_{MF_u}$, to ensure that the fMS $\hat{i}$ meets signal to interference power ratio (SIR) $\geq \Upsilon_{\hat{i}}$, the distance between mBS M and fMS $\hat{i}$ has to satisfy

$$|x_{M\hat{i}}| > \left(\frac{\Upsilon_{\hat{i}} P_{\mathrm{mBS}} K_m |x_{i\hat{i}}|^{\beta} W L^{-1}}{P^{\mathrm{fBS}}_{\hat{i}} K_f} \right)^{1/\alpha}. \quad (7)$$

According to Table 4 (see Section IV and related references), P_{mBS} is 10 to 100 times more than $P^{s-\max}_{\mathrm{fBS}}$ according to [4] and $K_m \gg K_f$. For clear expression, the relationship between P_{mBS} and $P^{\mathrm{fBS}}_{\hat{i}}$, and the relationship between d_{of} and $|x_{i\hat{i}}|$ are stated as

$$P_{\mathrm{mBS}} = \eta_{\hat{i}} P^{\mathrm{fBS}}_{\hat{i}} \quad (8)$$

and

$$d_{of} = \frac{|x_{i\hat{i}}|}{n_{i\hat{i}}}, \quad (9)$$

respectively, where $\eta_{\hat{i}}$ and $n_{i\hat{i}}$ are both scale factors. Substituting (5), (6), (8), and (9) into (7), we get

$$|x_{M\hat{i}}| > \left(\Upsilon_{\hat{i}} \eta_{\hat{i}} n^{\beta-2}_{i\hat{i}} d^{\alpha-2}_{om} |x_{i\hat{i}}|^2 W L^{-1} \right)^{1/\alpha}. \quad (10)$$

Due to the existence of $I^D_{MF_u}$, it is impossible to share the spectrum between femtocells and the macrocell within a certain minimum distance from the mBS. This conclusion is confirmed by the result of simulations in Section IV.

2) $I^D_{FF_u}$ (fBS co-channel interference at fMS): Assuming fMS $\hat{i}$ in femtocell i ($i \in S_F$) uses the same subchannel as fMS $\hat{j}$ in femtocell j ($\hat{j} \in S_{Fu,j}, j \in S_F$ and $i \neq j$), $I^D_{FF_u}$ can be written as $I^D_{FF_u} = \sum_{i \in I_1} P^{\mathrm{fBS}}_{\hat{i}} K_m |x_{i\hat{j}}|^{-\alpha} \chi_{i\hat{j}} W L^{-2}$, where I_1 is the set of fBSs that interfere with fMS $\hat{j}$. As can be seen from the expression of $I^D_{FF_u}$, the greater the number and the density of the femtocells, the stronger is the interference between them.

3) $I^D_{FM_u}$ (fBS interference at mMS): Assuming fMS $\hat{i}$ in the femtocell i ($i \in S_F$) using the same subchannel with mMS k ($k \in S_M$), $I^D_{FM_u}$ can be written as $I^D_{FM_u} = \sum_{i \in I_2} P^{\mathrm{fBS}}_{\hat{i}} K_m |x_{ik}|^{-\alpha} \chi_{ik} W L^{-1}$, where I_2 is the set of fBSs that interfere with mMS k. The signal received by mMS k from its serving mBS M can be denoted as $S^D_m = P_{\mathrm{mBS}} K_m |x_{Mk}|^{-\alpha} \chi_{Mk}$. By comparing $I^D_{FM_u}$ with S^D_m, it is easy to see that in the region of the macrocell edge (i.e., $|x_{Mk}|$ tending towards R_M), mMSs in the vicinity or coverage of the femtocell cannot share the spectrum with the femtocell (i.e., $|x_{ik}|$ tending towards or smaller than R_f), which is also proved in [11]. As indicated in Fig. 1(a), this region is referred to as the mMS downlink dead zone [1].

Based on the analysis of the downlink interference scenarios, two conclusions can be drawn.

- The mBS interference at fMSs and the fBS interference at mMSs lying in the vicinity or coverage of femtocells are the decisive restrictions for the frequency reuse between the macrocell tier and the femtocell tier.
- The fBS interference at fMSs in its neighboring femtocells[1] is the main restrictive factor for frequency reuse among femtocells.

The uplink interference scenario, shown in Fig. 1(b), can be quantitatively analyzed in the same way as the downlink interference scenario. Due to space limitations, the following conclusions are presented without quantitative analysis.

1) $I^U_{F_uM}$ (fMS interference at the co-channel mMS): $I^U_{F_uM}$ is caused by femtocells reusing subchannels with mMS in the same macrocellular coverage. $I^U_{F_uM}$ could skyrocket the interference to co-channel mMSs, especially when the mMS is located at the edge of the macrocell and co-channel femtocells are near the mBS, which corresponds to the case of $I^D_{MF_u}$.
2) $I^U_{F_uF}$ (the fMS interference at its co-channel fMS in the neighboring femtocell): It is obvious that the greater the number and density of femtocells, the stronger is the interference among them—which corresponds to the case of $I^D_{FF_u}$.
3) $I^U_{M_uF}$ (the mMS interference at the co-channel fMS in its neighboring femtocell): As shown in Fig. 1(b), there is an fMS uplink dead zone corresponding to the mMS downlink dead zone. This is incurred by the mMSs' higher transmit power needed by the nMSs in order to satisfy long distance transmission when non-CSG mMSs are located in the coverage area of the femtocell.

From the above analysis, it is obvious that the interference relationship between the uplink and the downlink is dual, that is, $I^U_{F_uM}$, $I^U_{F_uF}$, and $I^U_{M_uF}$, are the counterparts of the major downlink interference, that is, $I^D_{MF_u}$, $I^D_{FF_u}$, and $I^D_{FM_u}$.

Due to space limitations, the following work exclusively focuses on the downlink in the FMOS. However, the duality in the interference relationship between the uplink and the downlink interference scenarios results in portions of our analysis also being applicable to the uplink.

III. JFCPA

Based on the analysis of the FMOS interference scenario, the JFCPA is proposed in this section. First, two definitions are given.

Definition 1 (ISA): The area of the macrocell, where the transmit power per subchannel of the fBS reaches its upper bound—i.e., $P^{s-\max}_{\mathrm{fBS}}$, the target SIR of its serving fMS still can not be met—is defined as the ISA. The other area of the macrocell is defined as the NISA.

ISA and NISA are logical areas determined by the distribution and location of the femtocells.

Definition 2 (clustering threshold distance R_{th}): Considering only the co-channel interference in the femtocell tier, the minimum distance between two co-channel femtocells, within which the lowest target SIR for any fMS can be met, is defined as

[1] Hereafter, A neighboring B means that the coverage areas of A and B overlap.

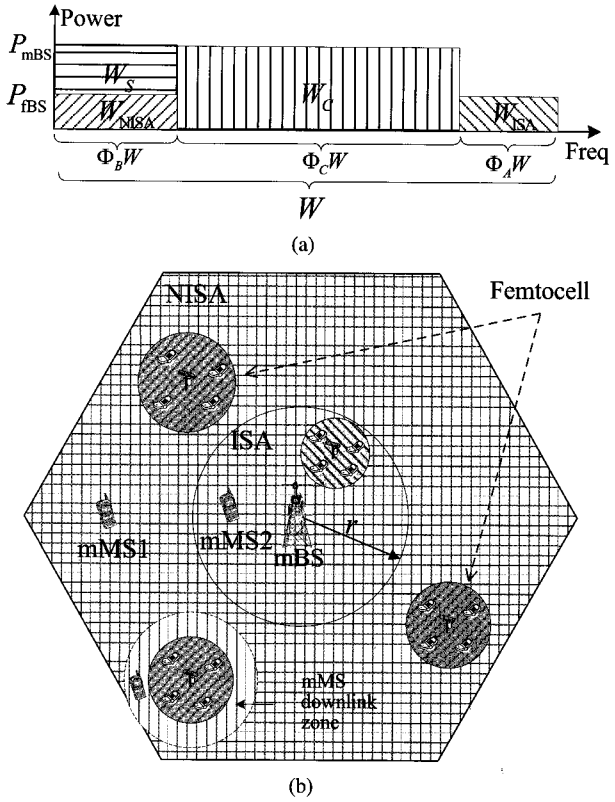

Fig. 2. Region and bandwidth divided by the JFCPA: (a) System frequency bandwidth division and (b) macrocell region division.

the clustering interference threshold distance. The mathematic derivation of R_{th} is given in Appendix A.

In addition, when the distance between femtocells is less than R_{th}, the inter-femtocell interference is referred to as the collision interference.

A. Target of the JFCPA

The target of the JFCPA is indicated in Fig. 2. The system frequency bandwidth and the macro cellular area are adaptively divided by the JFCPA. As shown in Fig. 2(b), mBS is taken as the coordinate of the origin. For the femtocell tier, the central circular area[2] is the ISA; the other area, the NISA. Fig. 2(a) shows the division of the entire bandwidth, W. W_{ISA} is the femtocell dedicated band, which is dedicatedly reused by the femtocell tier (including femtocells in NISA and ISA). To avoid intense $I^D_{MF_u}$ in ISA, femtocells in ISA can only reuse W_{ISA}. W_{NISA} and W_S are reused by femtocells in NISA and its home macrocell with different power, respectively. W_C is the macrocell dedicated band, which is allocated to guarantee the service quality of mMSs in the mMS downlink dead zone. The ratios of W_{ISA}, W_{NISA}(or W_S), and W_C are Φ_A, Φ_B, and Φ_C, respectively.

The system bandwidth of the OFDMA is divided into orthogonal subcarriers, which are in turn combined into groups, known as resource blocks or subchannels [14], [19]. In the JFCPA, different subchannels belonging to W_{ISA} and W_{NISA} are assigned to different clusters, whereas the same subchannels are reused among femtocells belonging to the same cluster.

[2]Here, we use a circular area to represent ISA as it more clearly illustrates the concept.

B. Main Procedure of the JFCPA

The main procedure of the JFCPA contains three major steps, which are implemented for NISA and ISA separately. In the following text, JFCPA implemented for NISA is taken as an example.[3] Hereafter, $\mathbb{R}'_l(l = 1, \cdots, \mathbb{N})$ denotes the set of femtocell clusters, where $\mathbb{N}$ is the cardinality of clusters. $\mathbb{N}$ can be divided into the cardinality of cluster in ISA and that in NISA, which are denoted $\mathbb{N}_{\mathrm{ISA}}$ and $\mathbb{N}_{\mathrm{NISA}}$, respectively. The number of femtocells in $\mathbb{R}'_l$ is denoted as N_l.

The main procedure of the JFCPA for NISA is described in detail as follows.

Step 1: Utilizing R_{th}, construct the femtocell interference graph G and its adjacent matrix $A(G)$ to map the clustering problem into a graph problem.

Step 2: Apply the adaptive clustering heuristic algorithm (ACHA) to assign femtocells into cluster sets $\mathbb{R}'_l(l = 1, \cdots, \mathbb{N}_{\mathrm{NISA}})$, where $\mathbb{N}_{\mathrm{NISA}}$ is the cardinality of the cluster set $\mathbb{R}'_l$ in NISA.

Step 3: Step migration algorithm (SMA) based power control.

1) Construct linear inhomogeneous equations subject to target signal to interference and noise ratios (SINRs) of all femtocells in $\mathbb{R}'_l$ and calculate fBSs' transmit power.
2) According to fBSs' transmit power solutions, operate SMA to make corresponding femtocell(s) migrate from current cluster $\mathbb{R}'_l$ to cluster $\mathbb{R}'_{l+1}$ or to the femtocell set of ISA (S_{ISA}), and then return to step 3.1) until $l = \mathbb{N}_{\mathrm{NISA}}$.

In the following subsections, the three steps of the JFCPA are described in detail: Step 1 (i.e., the clustering algorithm) is depicted in subsections III.C and III.D; step 2 (ACHA based on interference graph) is described in subsection III-E; step 3 (i.e., SMA-based power control) is presented in subsection III.F.

C. Clustering Problem

Because the frequency resource available is limited, it has to be reused for densely deployed femtocells. In this paper, the resource reuse unit of femtocells is the cluster. Therefore, the objective of clustering femtocells should avoid collision interference between femtocells and minimize the co-channel interference of every femtocell in the same cluster. The distance between femtocells is one of the deterministic factors that reflect the interference in ISA and the co-tier interference power received by fMSs in NISA. To control the cross-tier interference in NISA, femtocell clusters are further adjusted by SMA-based power control. Here, the clustering problem is constructed as

$$\begin{aligned} \max \quad & \sum_{l=1}^{\mathbb{N}} \sum_{i,j \in \mathbb{R}'_l, i \neq j} d_{ij} \\ \text{s.t.} \quad & d_{ij} - R_{th} > 0 \\ & \bigcup_{l=1}^{\mathbb{N}} \mathbb{R}'_l = S_F \\ & \mathbb{R}'_m \cap \mathbb{R}'_n = \text{Null} \qquad m \neq n, \quad m, n \in [1, \mathbb{N}] \end{aligned} \tag{11}$$

[3]The difference between JFCPA to NISA and ISA is in step 3, which is explained in subsection III.F.

Table 2. Construction procedure for adjacent matrix of interference graph.

Initializations:
Define $\Re_{\mathbf{th}} = [\mathbf{R_{th}}]_{\mathbf{N}\times\mathbf{N}}$, where N is the cardinality of S_F.
'$\otimes$' represents the Kronecker product.
$\mathbf{\Psi}$ is an $N\times N$ matrix consisting only of ones.
$\mathbf{I}$ is an $N\times N$ identity matrix; $\mathbf{D} = [\mathbf{d_{ij}}]_{\mathbf{N}\times\mathbf{N}}$.
1: Calculate matrix $\mathbf{Q}$ as
2: $\quad \mathbf{Q} = \mathbf{D} - \Re_{\mathbf{th}} \otimes (\mathbf{\Psi} - \mathbf{I})$
3: For all entries in $\mathbf{Q}$
4: $\quad$ If $d_{ij} - R_{th} < 0$, then
5: $\quad\quad a(\nu_i, \nu_j) = 1$
6: $\quad$ Else
7: $\quad\quad a(\nu_i, \nu_j) = 0$
8: $\quad$ End
9: End
10: $\mathbf{A(G)} = [\mathbf{a}(\nu_\mathbf{i}, \nu_\mathbf{j})]_{\mathbf{N}\times\mathbf{N}}$ is obtained.

where $d_{ij} = \sqrt{(x_i - x_j)^2 + (y_i - y_j)^2}$ is the distance between femtocell i and femtocell j which are located at (x_i, y_i) and (x_j, y_j), respectively; S_F is the set of all femtocells; and $\mathbb{N}$ is the cardinality of the cluster set. As seen from (11), any two femtocells, between which the distance is less than R_{th}, must be assigned to different clusters in order to avoid collision interference.

The clustering problem (11) has the same model as the MAX k-CUT problem, which has been proved to be an nondeterministic polynomial-time hard (NP-hard) problem [20]. Therefore, the suboptimal heuristic algorithm is often adopted to solve the problem [20]–[22]. However, these algorithms are based on the premise that the number of clusters is predetermined and fixed, which reduces the spectrum efficiency of FMOS, especially when femtocells are sparsely distributed. As a result, ACHA based on graph method is proposed in this study. This graph method is composed of two steps: Construction of femtocell interference graph and ACHA based on the interference graph.

D. Construction of the Femtocell Interference Graph

In accordance with the definition of a graph in the graph theory [23], the femtocell interference graph is represented as $G = (V, E)$, where V is the set of vertices and E is the set of edges. Each femtocell i in S_F is regarded as a vertex, i.e., $\nu_i, \forall i \in S_F$. In a similar vein, E represents the edge formed by the joining of ν_i and ν_j, i.e., $e(\nu_i, \nu_j), \forall i, j \in S_F$, which reflects the interference collision relationship between femtocells. Concretely speaking, if the distance between any two femtocells i and j $(i, j \in S_F, i \neq j)$ is less than R_{th}, $e(\nu_i, \nu_j)$ exists between the corresponding vertices ν_i and ν_j. In order to quantitatively represent the interference graph G, the adjacent matrix of G, the adjacent matrix of G, denoted as $\mathbf{A(G)} = [\mathbf{a}(\nu_\mathbf{i}, \nu_\mathbf{j})]_{\nu_\mathbf{i}\in\mathbf{V}, \nu_\mathbf{j}\in\mathbf{V}}$, is constructed.

The procedure for constructing the adjacent matrix of interference graph G is presented in Table 2.

Due to the nonexistence of interference between the fMS and their serving fBS, there is no loop in the interference graph. Let $d_G(\nu_i)$ represent the degree of vertex ν_i in the interference graph. Then, the vertices in V have the following properties.

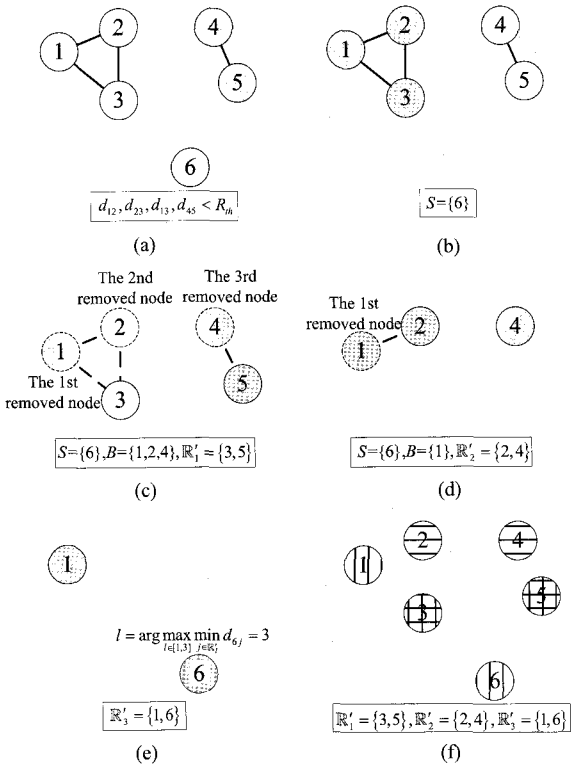

Fig. 3. An example of clustering femtocells: (a) Femtocell interference graph, (b) removing the 0 degree vertex, (c) cluster the 1st cluster, (d) reconstruct interference graph and cluster the 2nd cluster, (e) cluster the 3rd cluster, and (f) ACHA cluster result.

Property 1: If $d_G(\nu_i) = 0$, ν_i is an isolated vertex, which means that there is no collision interference between the corresponding femtocell i and any other femtocell.

Property 2: If $d_G(\nu_i) \neq 0$, there is collision interference among the corresponding femtocell i and femtocells whose corresponding vertices (i.e., $\nu_j, j \in S_F, j \neq i$,) connect with ν_i. In addition, the greater $d_G(\nu_i)$ is, the more is the collision interference experienced by the corresponding femtocell i.

The following example 1 below exemplifies the construction of the adjacent matrix of the interference graph.

Example 1: Femtocell interference graph and its adjacent matrix.

Assuming 6 femtocells distributed as shown in Fig. 3(a), with distance relation $d_{12}, d_{23}, d_{13}, d_{45} < R_{th}$. By applying the construction rule in Table 2 to the example, the femtocell interference graph is constructed as Fig. 3(a), and its resulting adjacent matrix is

$$\begin{bmatrix} 0 & 1 & 1 & 0 & 0 & 0 \\ 1 & 0 & 1 & 0 & 0 & 0 \\ 1 & 1 & 0 & 0 & 0 & 0 \\ 0 & 0 & 0 & 0 & 1 & 0 \\ 0 & 0 & 0 & 1 & 0 & 0 \\ 0 & 0 & 0 & 0 & 0 & 0 \end{bmatrix}. \tag{12}$$

E. ACHA Based on Interference Graph

In ACHA, the number of clusters is adaptively determined by the distribution of femtocells. More concretely, vertices of

Table 3. Description of ACHA.

Initializations:
Let integer l be the index of the cluster with initial value 1.
Let S and B be an isolated vertex set and a temporary storage set, respectively.

1: $\mathbf{A_1(G)} = \mathbf{A(G)}$
2: For all ν_i in V %Remove all 0 degree vertices
3: If $d_G(\nu_i) = 0$, then
4: Remove ν_i from $\mathbf{A_1(G)}$
5: Record ν_i into the isolated set, i.e., $S \Leftarrow \nu_i$
6: End
7: End
8: Make $\mathbb{R}'_l = V - S$
9: While $\mathbf{A_1(G)}$ is not the zero matrix
10: Do %Cluster one cluster
11: $i = \arg\max_i (d_G(\nu_i))$
12: Remove ν_i from $\mathbf{A_1(G)}$
13: Exclude ν_i from $\mathbb{R}'_l$ and record ν_i to B
14: Until $\mathbf{A_1(G)} = \mathbf{0}$
15: Increment l and make $\mathbb{R}'_l = B$
16: Utilize B to reconstruct $\mathbf{A_1(G)}$ as outlined in Table 2
17: Clear set B
18: End
19: Make $\mathbb{N} = l$
20: Arbitrarily order isolated vertices in S
21: Allocate every vertex in S to cluster $l^* = \arg\max_{l\in[1,\mathbb{N}]} \min_{j\in\mathbb{R}'_l} d_{ij}$

$d_G(\nu_i) \neq 0$ determine the number of clusters and are allocated to clusters according to the interference graph G. As a result, the cluster index of isolated vertices is obtained using $l^* = \arg\max_{l\in\{1,2,\cdots,\mathbb{N}\}} \min_{j\in\mathbb{R}'_l} d_{ij}$.

Definition 3 (operation rule for removing the vertex in $\mathbf{A(G)}$) : In ACHA, delete the row and column corresponding to the vertex removed from $\mathbf{A(G)}$ and reserve the other elements (including values and relationship) to form a new matrix.

For example, let the adjacent matrix, that is, $\mathbf{A}$, of three vertices be

$$\begin{bmatrix} a_{11} & a_{12} & a_{13} \\ a_{21} & a_{22} & a_{23} \\ a_{31} & a_{32} & a_{33} \end{bmatrix}. \quad (13)$$

When vertex 1 is removed, matrix $\mathbf{A}$ becomes

$$\begin{bmatrix} a_{22} & a_{23} \\ a_{32} & a_{33} \end{bmatrix}.$$

ACHA is described in Table 3. Example 2 below exemplifies ACHA.

Example 2: Operating ACHA to cluster femtocells.

Following the result of example 1, Fig. 3(b) indicates that the zero degree vertex (vertex 6) is removed and placed in set S, and the interference graph is reconstructed. Fig. 3(c) indicates that vertices 1, 2, and 4 are removed and placed in set B, resulting in only vertices 3 and 5 comprising the first cluster, that is, $\mathbb{R}'_1 = \{3, 5\}$. Using the elements of set B, the new femtocell interference graph is constructed as shown in Fig. 3(d). Next, vertex 1 is removed from the reconstructed graph and placed in set B: This results in vertices 2 and 4 comprising the second cluster, that is, $\mathbb{R}'_2 = \{2, 4\}$. From Fig. 3(e), it is clear that the degrees of all the vertices in the reconstructed graph are zero. As a result, the third cluster is constructed with vertex 1. Because $l = \arg\max \min_{l\in\{1,2,3\}, j\in\mathbb{R}'_l} d_{6j} = 3$, the third cluster is renewed as $\mathbb{R}'_3 = \{1, 6\}$. Finally, the clustering result is shown with a different fill pattern in Fig. 3(f).

F. SMA-Based Power Control

The power control algorithm in this paper is based on Bambos's algorithm [24]–[27] and Zander's algorithm [28], which are both based on linear inhomogeneous subject to all users' target SINR similar to (15). To solve these equations, Bambos's algorithm uses Gaussian elimination or iterative algorithms, which are computationally burdensome when there are an increasing number of users. Zander's algorithm uses an SIR balancing scheme that makes all users achieve the same maximum SIR. The SIR balancing scheme maximizes the worst SIR, but may fall short of the required higher SIR. In addition, the SIR balancing scheme neglects the right hand side (RHS) constant term of linear inhomogeneous equations, which is incurred by Gaussian noise. When interference is much greater than Gaussian noise, it is rational. However, in the case of FMOS, the RHS constant term is incurred by Gaussian noise and interference from the mBS that can be much greater than the left hand side (LHS) term incurred by the interference between femtocells, as presented in (15). Therefore, the RHS constant term in FMOS equations can not be neglected. This fact is also evident from the following detailed analysis.

Further, because some solutions of these two algorithms may be out of the valid solution range, there have already been some strategies that remove some users to make the power allocation of the remaining users satisfy the power constraints, for example, the stepwise removal algorithm (SRA) [28]. However, these algorithms are not feasible in situations where there are multiple major interferences, for example, FMOS.

To solve the above mentioned problems, we propose the SMA-based power control algorithm that has been described in detail below.

Because a femtocell is taken as the unit for quality of service (QoS) differentiation as mentioned in assumption 3, SMA-based power control only needs to allocate the minimal transmit power to every fBS on the premise of meeting the fMS's SINR requirement in any position of the femtocell. In order to determine the minimal transmit power, we consider the worst-case scenario. This scenario occurs when the reference fMS lies at the edge of the femtocell and nearest to the mBS. Therefore, the power solution in this worst-case scenario could meet the QoS requirement of all fMSs at any position within the femtocell area range. In order to guarantee the required SINR for the reference user in femtocell i of cluster $\mathbb{R}'_l$, the following relation must hold[4]

[4]Because the reference fMS has been introduced, the index of the femtocell can be used for the index of the reference fMS.

$$\Upsilon_i = \frac{P_i^{\text{fBS}} G_{ii}^{f1}}{\sum_{\substack{j \in \mathbb{R}_l' \\ j \neq i}} P_j^{\text{fBS}} G_{ij}^{f2} + P_{\text{mBS}} G_{Mi}^{m2} + N_0} \tag{14}$$

where G_{Mi}^{m2} and G_{ij}^{f2} are path gains between the mBS and femtocell i, and between femtocell i and its interfering femtocells, respectively; G_{ii}^{f1} is the path gain between the reference fMS and its serving fBS; Υ_i is the required SINR for femtocell i in cluster $\mathbb{R}_l'$, which is the function of the applied modulation level and the required bit error rate [29]; P_i^{fBS} and P_{mBS} are the fBS and mBS transmit power, respectively, of the subchannel allocated to the reference fMS in cluster l; and N_0 is the noise power of each subchannel. Rearranging (14) leads to the following linear equation[5]

$$P_i - \Upsilon_i \sum_{\substack{j \in \mathbb{R}_l' \\ j \neq i}} P_j \frac{G_{ij}^{f2}}{G_{ii}^{f1}} = \frac{\Upsilon_i}{G_{ii}^{f1}} N_0 + \frac{\Upsilon_i G_{Mi}^{m2}}{G_{ii}^{f1}} P_{\text{mBS}}. \tag{15}$$

This generalized equation applied to all femtocells in cluster $\mathbb{R}_l'$, yields the following matrix equation

$$(\mathbf{I} - \mathbf{H})\mathbf{P} = \mathbf{N_0}\boldsymbol{\Upsilon} + \mathbf{P}_{\text{mBS}}\hat{\boldsymbol{\Upsilon}} \tag{16}$$

where

$$\mathbf{H} = \begin{bmatrix} 0 & \frac{G_{12}^{f2}}{G_{11}^{f1}}\Upsilon_1 & \cdots & \frac{G_{1,N_l}^{f2}}{G_{11}^{f1}}\Upsilon_1 \\ \frac{G_{21}^{f2}}{G_{22}^{f1}}\Upsilon_2 & 0 & \cdots & \vdots \\ \vdots & \vdots & \ddots & \vdots \\ \frac{G_{N_l,1}^{f2}}{G_{N_l,N_l}^{f1}}\Upsilon_{N_l} & \cdots & \cdots & 0 \end{bmatrix}, \tag{17}$$

$$\mathbf{P} = [P_1, P_2, \cdots, P_{N_l}]^T, \tag{18}$$

$$\boldsymbol{\Upsilon} = \left[\frac{\Upsilon_1}{G_{11}^{f1}}, \frac{\Upsilon_2}{G_{22}^{f1}}, \cdots, \frac{\Upsilon_{N_l}}{G_{N_l,N_l}^{f1}}\right]^T, \text{ and} \tag{19}$$

$$\hat{\boldsymbol{\Upsilon}} = \left[\frac{\Upsilon_1 G_{M1}^{m2}}{G_{11}^{f1}}, \frac{\Upsilon_2 G_{M2}^{m2}}{G_{22}^{f1}}, \cdots, \frac{\Upsilon_{N_l} G_{M,N_l}^{m2}}{G_{N_l,N_l}^{f1}}\right]^T. \tag{20}$$

Methods for solving (16) have been discussed in [24] and [26]. This paper focuses on the power solutions beyond the valid range $[0, P_{\text{fBS}}^{s-\max}]$, which provides useful information to determine the femtocell set of ISA, and to adjust the assignment of femtocells among clusters so as to reduce the probability of outages and transmit powers of fBSs. Based on the power solutions obtained at each round of solving the linear equations, SMA for NISA is determined as follows.

Let the power solution vector of cluster $\mathbb{R}_l'$ be $\mathbf{P} = [P_k], 1 \leq k \leq N_l$. At each round in the solution of the linear equations,

1) the femtocells, in which the transmit power satisfies $|P_k| > P_{\text{fBS}}^{s-\max}$, migrate from cluster $\mathbb{R}_l'$ to the ISA femtocell set S_{ISA};

2) if any $P_k \in \left(-P_{\text{fBS}}^{s-\max}, 0\right)$ exists, the femtocell with the maximum sum of row and column

$$\arg \max_{i \in [1, N_l]} \left\{ \sum_{j=1}^{N_l} \Upsilon_i \frac{G_{ij}^{f2}}{G_{ii}^{f1}} + \sum_{j=1}^{N_l} \Upsilon_j \frac{G_{ji}^{f2}}{G_{jj}^{f1}} \right\} \tag{21}$$

migrates from cluster $\mathbb{R}_l'$ to cluster $\mathbb{R}_{l+1}'$.

Proof and analysis: see Appendix B and C.

SMA-based power control for ISA, consists of only the power control algorithm mentioned above and SMA 2) due to the nonexistence of $I_{MF_u}^D$ in ISA.

A complexity analysis of Bambos's algorithm has already been analyzed in [26]. In the current paper, we want to clarify that the SMA-based power control algorithm reduces the computational complexity by at least $\mathbb{N}$ times when Bambos's algorithm is of complexity $O(m^2)$ for m users. This is due to the fact that a cluster is taken as the unit for power control in the proposed algorithm.

Implementation of the JFCPA is primarily related to factors that consider position changes and on/off switches in fBSs. Variation of these factors is relatively slow when compared with wireless channel variation. Therefore, the JFCPA can be implemented in a relatively large time unit. Moreover, as the position of fMSs is relatively fixed and the number of fMSs is very small in the home area, further transmit power allocation for fMSs in the same femtocell can be operated autonomously by the fBS. The effectiveness of the JFCPA in terms of interference control, user capacity, spectrum efficiency, and power reduction is evaluated in the subsequent section.

IV. PERFORMANCE EVALUATION

System simulation parameters obtained from [4] and [14] are listed in Table 4. In the simulation, femtocells were randomly placed in a macrocell. Every femtocell contained four active fMSs. In the macrocell tier, 20 mMSs were randomly placed within the macrocell coverage area. All the available subchannels transmitted with equivalent power, in accordance with [14], and the scheduler for the mBS ensured proportional, fair resource allocation. The simulation exercise had four objectives. The first was to verify the existence of ISA and the effectiveness of SMA. The second was to simulate the performance of the JFCPA. The third was to compare the results of the JFCPA to Bambos's power control algorithm combined with SRA (hereafter, short for Bambos's algorithm). The fourth was to provide the throughput gain of the JFCPA and compare its performance to two other schemes.

A. Simulation for Existence of ISA and Effectiveness of SMA

In this subsection, two simulations are operated in the same shadow-loss scenario. Fig. 4(a) was obtained by traversing the entire macrocell with 15000 femtocells. The corresponding femtocell was marked by a gray circle if the SINR requirement of reference fMSs could be satisfied within the valid transmit power range (i.e., $[0, P_{\text{fBS}}^{s-\max}]$); otherwise, it was not marked. The central white area in Fig. 4(a) is the ISA, which was also proved by (10). The JFCPA was applied in 100 different scenarios, each of which contained 150 randomly placed femto-

[5]Hereafter, P_i is used to stand for P_i^{fBS} as it is clear from the context.

Table 4. System simulation parameters.

Simulation parameter	Value
R_M, R_f (m)	500, 20
$P_{\mathrm{mBS}}^{\max}$, $P_{\mathrm{fBS}}^{\max}$ (dBm)	43, 20
Active fMSs per femtocell	4
Number of subchannels	30
FFT size, active FFT size	2048, 1440
DL permutation Type	Partially used sub-carrier
d_{om}, d_{of} (m)	5, 100
α, β	4, 2.5
f_c (GHz)	2
σ_B (dB)	6
Penetration loss (dB)	10
fMS target SINR Υ_i (dB)	[3,10]
mMS target SINR (dB)	10
Fast fading	Spatial channel model [30]

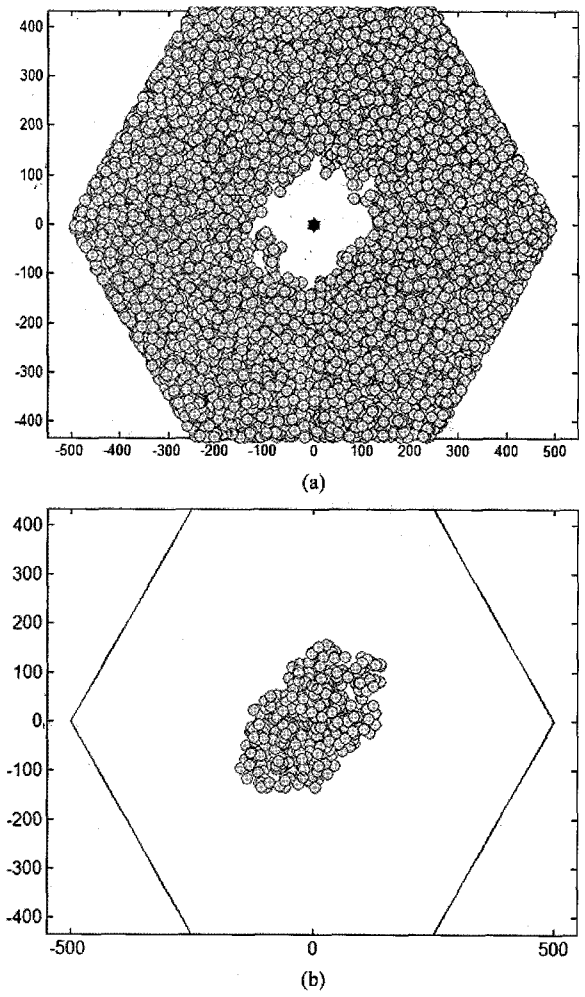

Fig. 4. Simulation results of ISA and NISA division.

cells. The simulation result shows that SMA-based power control identifies femtocells belonging to the ISA (marked in the central area). The shadow-loss contour of the simulation scenario leads to the shape of the ISA oval. This comfirms the existence of ISA and the effectiveness of the SMA algorithm.

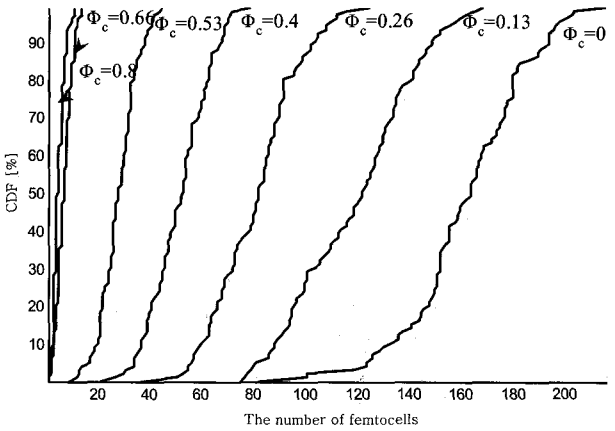

Fig. 5. Femtocell maximum number statistical result in one macrocell coverage with varying Φ_C.

B. Performance of the JFCPA

Figs. 5, 6, and 7 graphically illustrate the performance of the JFCPA. Fig. 5 shows the cumulative distribution function (CDF) of the femtocell-tier capacity in one macrocell coverage with varying Φ_C, that is, the ratio of the macrocell dedicated band. Fig. 6 shows the ratios of the different bands with varying Φ_C. By analyzing these two simulation results together, the following conclusions can be drawn.

- When the entire system frequency resource is available to the femtocell tier, that is, $\Phi_C = 0$, the number of femtocells in one macrocell coverage distributes mainly between 140 and 180, and reaches a maximum of 219. However, the ratio of the FMOS reuse band, i.e., Φ_B, is still greater than 70%, which means that more than 70% of the overall frequency bandwidth is available to the macrocell tier.
- The ratio of the frequency band available to the macrocell tier (i.e., $\Phi_C + \Phi_B$) increases linearly with an increase in Φ_C. Furthermore, when $\Phi_C > 66\%$, the entire system frequency resource is available to the macrocell tier, that is, $\Phi_C + \Phi_B = 100\%$.
- Within the frequency band available to the femtocell tier, the ratio of the FMOS reuse band, that is, Φ_B, is 40% more than the ratio of the femtocell dedicated band, Φ_A; in other words, the femtocell dedicated band is only 30% of the frequency band available to the femtocell tier. Therefore, no matter how much frequency band is assigned to the femtocell tier, there is at least 70% of the system frequency bandwidth available to the macrocell tier.
- The random distribution of femtocells may result in femtocell-dense distribution areas, where the distances among a large number of femtocells are less than R_{th}, for example, the residential area, the official area, and the like, in actual deployments.

Lemma 1: A simple graph holds for $\omega \leq \chi \leq \Delta + 1$, where χ is the chromatic number of the interference graph G; ω is the number of vertices of the maximal clique in G; and Δ is the number of the maximal degree of G [31].

From Lemma 1, increasing the required chromatic number of the interference graph G leads to more clusters. Therefore, the frequency resources allocated to the femtocell tier is easily to be exhausted, especially when a small portion of the frequency

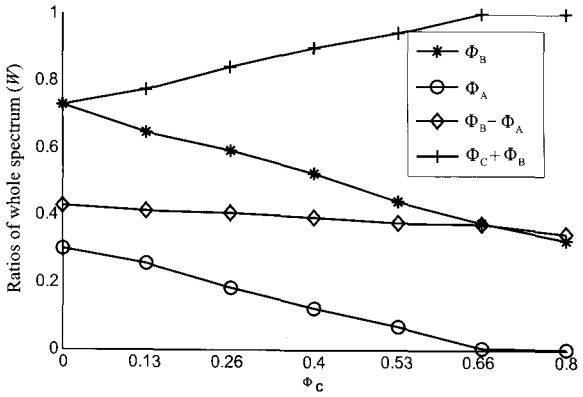

Fig. 6. Ratios of different bands in W to varying Φ_C.

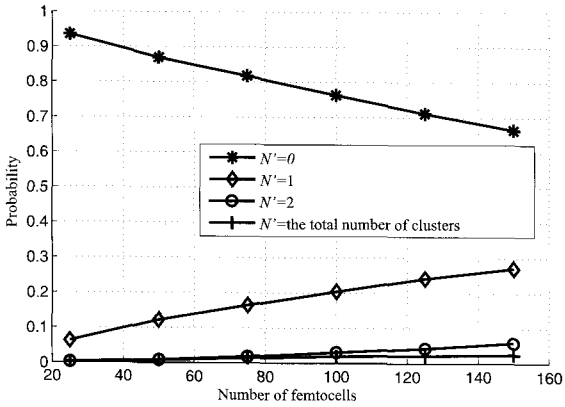

Fig. 7. Probability of mMS lying in dead zone in proportion to the number of femtocells.

resource is available to the femtocell tier, that is, $\Phi_C = 0.8$ and $\Phi_C = 0.66$.

In order to evaluate the impact of the dead zone on the macrocell tier of the JFCPA, the probability of one mMS lying in the dead zone (or mMS collision with femtocell clusters) is computed using

$$\text{prob}\left(\mathcal{N} = N'\right) = \prod_{\mathcal{N}=1}^{N'} \left(\frac{\sum_{i \in \mathbb{R}'_{\mathcal{N}}} A_i^{DZ}}{A_M} \frac{1}{N_C} \right) \tag{22}$$

where A_M is the area of the macrocell; A_i^{DZ} is the area of the mMS downlink dead zone caused by the ith femtocell of the lth cluster; N_C is the number of subchannels allocated to each cluster; and $\mathcal{N}$ is defined as the random variable of the number of clusters. If $N' = 1$, (22) represents the probability of one fMS lying in the dead zone caused by one cluster, and the meaning of $N' > 1$ can be deduced by analogy.

Fig. 7 graphically illustrates the results obtained when (22) was utilized. When the number of femtocells reaches 150, the probability that the mMS will select a subchannel within the FMOS reuse band reaches 67%, while the probability that the mMS cannot use any subchannel within the FMOS reuse band is less than 2.4%, (that is, the probability that one mMS does not lie in the dead zone is above 97.6%), when any subchannel in the FMOS reuse band is utilized. Therefore, the JFCPA effectively reduces the probability of slow moving mMSs being trapped in

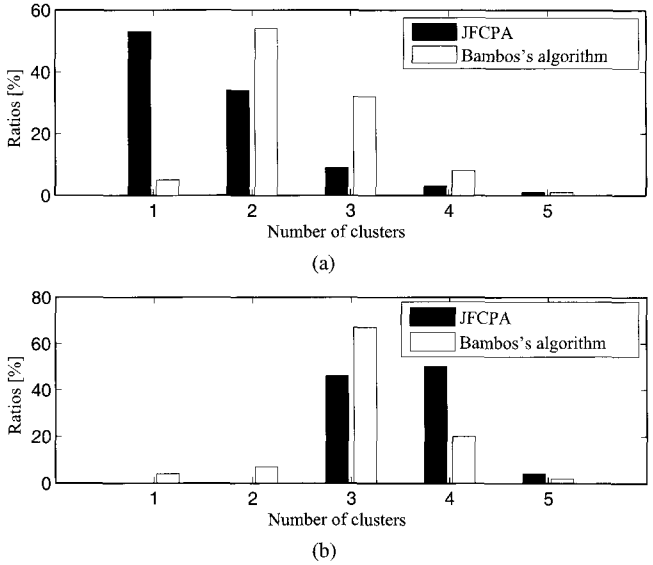

Fig. 8. Cluster number comparison between JFCPA and Bambos's algorithm using 150 femtocells: (a) ISA and (b) NISA.

the dead zone for extended periods of time. This is due to the fact that ACHA disperses femtocells more evenly into different clusters; thus, the femtocells in the same cluster are scattered more evenly, which can be seen from Fig. 10.

In conclusion, W_C is the fundamental factor in determining the capacity of the femtocell tier. These results provide a guideline for operators to adjust the ratio of three bands according to the traffic load of the macrocell and femtocell distribution density, either manually or adaptively.

C. Comparison of JFCPA and Bambos's Algorithm

Bambos's algorithm directly applies the methods in [24] and SRA [28] (i.e., SRA) to FMOS. The procedure used is as follows.

1) Compute the solution to (16) and remove certain femtocells from the current femtocell set according to SRA until the solution to (16) meets the maximum transmit power constraint.
2) Use the remaining femtocells to construct a cluster.
3) Repeat this procedure until until all femtocells obtain the required resources or all frequency resources are used up.

The results of the comparison between the JFCPA and Bambos's algorithm are shown in Figs. 8, 9, and 10. These figures were obtained by taking snapshots of 100 different scenarios using 150 femtocells. From Fig. 8, the following results were obtained.

- In NISA, the number of clusters of these two algorithms mainly distributes at 3 and 4. However, the 4-cluster ratio of the JFCPA is much higher than that of Bambos's algorithm; further, there is no single or double clusters for JFCPA. Bambos's algorithm is a "best effort" algorithm, in which the cluster is assigned with as many femtocells as possible. Therefore, the number of clusters it has is statistically less than that of the JFCPA in NISA.
- In ISA, the clusters for the JFCPA are primarily distributed in ones and twos, while those for Bambos's algorithm are

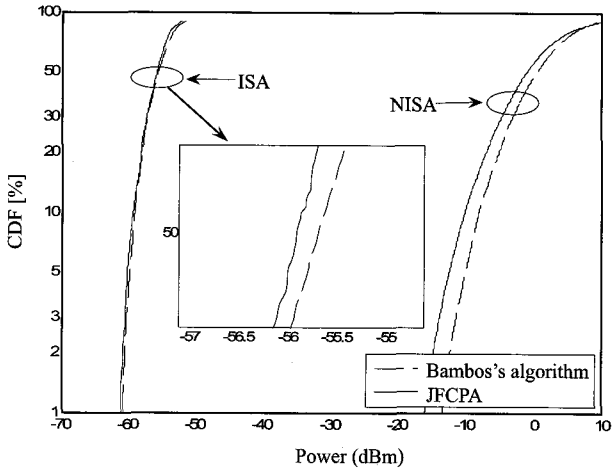

Fig. 9. P_{fBS} distribution of the JFCPA and Bambos's algorithm under the scenario of 150 femtocells.

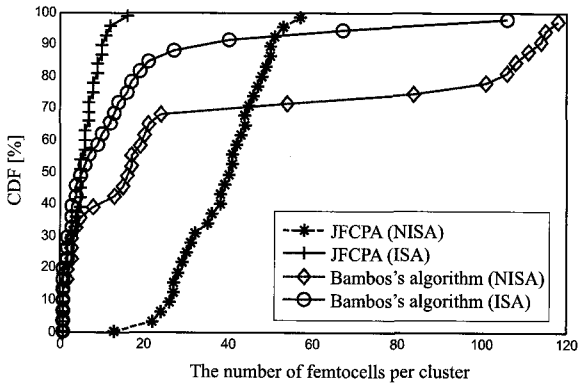

Fig. 10. Femtocell number per cluster distribution of the JFCPA and Bambos's algorithm under the scenario of 150 femtocells.

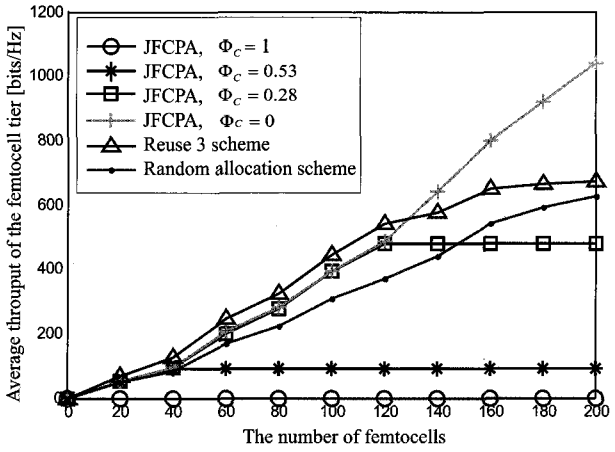

Fig. 11. The average throughput of the femtocell tier versus the number of femtocells.

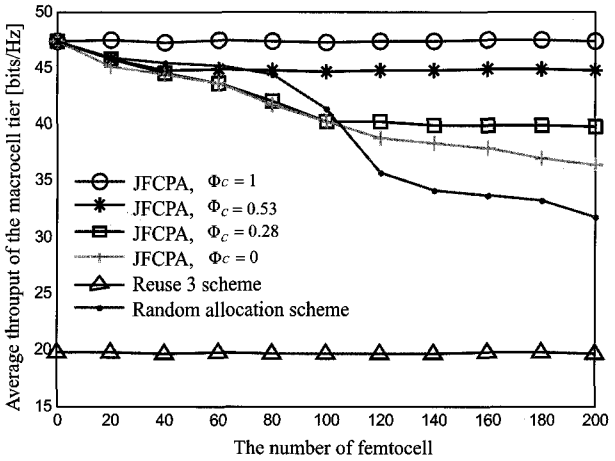

Fig. 12. The average throughput of mMSs versus the number of femtocells.

distributed in twos and threes. In addition, the total number of clusters for the JFCPA is clearly less than that for Bambos's algorithm. Because ACHA avoids collision interference among femtocells in each cluster, femtocells could endure greater interference from the mBS under the same SINR requirement. However, without consideration of balancing inter-femtocell interference among clusters in Bambos's algorithm (in JFCPA, balancing inter-femtocell interference among clusters is achieved by ACHA), there is great difference in the number and density of femtocells among clusters, as shown in Fig. 10. This makes femtocells in large-number clusters more sensitive to interference from the mBS, particularly those femtocells that are close to the mBS. Therefore, with Bambos's algorithm, more femtocells belong to ISA compared to the JFCPA, and thus its number of clusters in ISA can be more. This leads to the femtocell dedicated band ratio of Bambos's algorithm being greater than that of the JFCPA.

As shown in Fig. 9, the fBS transmit power of the JFCPA is lower than that of Bambos's algorithm under the same SINR requirement because the clustering procedure of the JFCPA mitigates inter-femtocell interference in every cluster.

As shown in Fig. 10, using the JFCPA, the number of femtocells in each cluster is evenly distributed: mainly between 25 and 50 for NISA and between 3 and 10 for ISA. Using Bambos's algorithm, the probability that the number of femtocells is over 100 is 30%, and the probability of the number being below 25 is close to 70%. This uneven distribution raises the probability of mMSs being trapped in the mMS dead zone and reduces the availability of the FMOS reuse band for mMSs. Therefore, the JFCPA results in better FMOS reuse band reusability.

D. Throughput Gain of the JFCPA

In order to compare the hybrid scheme with the universal frequency reuse scheme and the frequency partitioning scheme, two representative schemes of them were introduced.

Comparison scheme 1: Random allocation scheme [13].

In this scheme, each femtocell randomly selects an OFDMA subchannel for its fMS's transmission.

Comparison scheme 2: Reuse 3 scheme.

In this scheme, the system frequency reuse factor is 3, and the femtocell tier can only use 2/3 of the frequency bandwidth that is not allocated to its home macrocell.

In all three schemes being compared, every fBS applies power control autonomously to satisfy its home fMSs' SINR requirements, jointly considering the fast-fading, path-loss, penetration loss, and shadowing.

As shown in Figs. 11, 12, and 13, the throughput metrics of

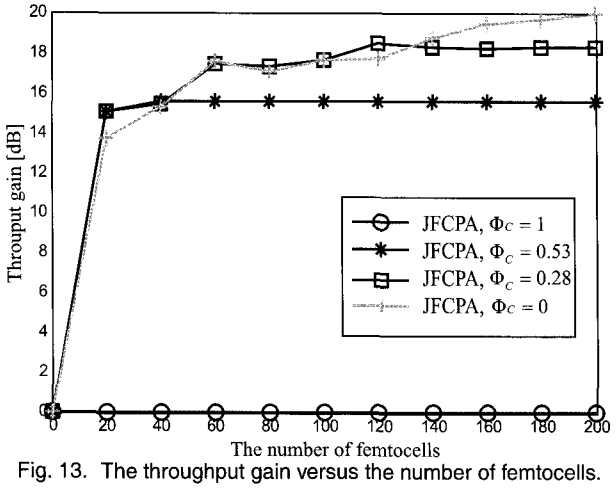

Fig. 13. The throughput gain versus the number of femtocells.

the JFCPA in the cases where $\Phi_C = 1$, $\Phi_C = 0.53$, $\Phi_C = 0.26$, and $\Phi_C = 0$ were evaluated and compared to both the reuse 3 scheme and the random allocation scheme.

Fig. 11 shows that for the femtocell tier, the higher the available bandwidth, the higher is the throughput that can be achieved. For the JFCPA, because the capacity of femtocells is determined by the frequency bandwidth allocated to the femtocell tier, the average throughput of the femtocell tier stops increasing when the number of femtocells reaches a certain number. For example, when $\Phi_C = 0.53$ and $\Phi_C = 0.26$, the breakpoints are 40 and 120, respectively. For the random allocation scheme, the throughput of the femtocell tier is smaller than that of the JFCPA, and the gap increases as the number of femtocell increases. This is due to the fact that subchannel random allocation does not exercise good control over the cross-tier and the co-tier interference. In the reuse 3 scheme, the cross-tier interference is totally eliminated at the expense of system spectral efficiency. When the number of femtocells is below 120, the throughput of the femtocell tier is slightly greater than that of the JFCPA with $\Phi_C = 0$. However, when the number of femtocell exceeds 120, the throughput of the femtocell tier is much lower than that of the JFCPA. This phenomenon is arises because the JFCPA mitigates the cross-tier and the co-tier interference properly, especially when a large number of femtocells are situated in proximity.

Fig. 12 illustrates how the average throughput of the macrocell tier varies as the number of femtocells increases from 0 to 200. For the JFCPA, when the macrocell tier uses the entire the system bandwidth, that is, $\Phi_C = 1$, the average throughput of the mMSs can be seen as a baseline. As Φ_C decreases, the throughput loss of the macrocell tier increases. However, due to the limited bandwidth allocated to the femtocell tier, only a limited number of femtocells can be served. Therefore, the performance of the macrocell tier does not further deteriorate when the number of femtocells reaches 40 and 120 for $\Phi_C = 0.53$ and $\Phi_C = 0.26$, respectively. When $\Phi_C = 0$ and the number of femtocells is 200, the average ratio of Φ_A is 29.5% (see Fig. 6). However, the highest loss of throughput is only 21%. This is due to the fact that frequency diversity in the macrocell tier brings throughput gain of mMSs. The throughput gain can also be obtained in other values of Φ_C. The throughput of the macrocell tier is lowest for the reuse 3 scheme. This is due to the fact that only $1/3$ of the frequency bandwidth is available to the macrocell tier. For the random allocation scheme, the throughput of the macrocell tier is lower than that of the JFCPA with $\Phi_C = 0$, when the number of femtocell exceeds 100. This phenomenon indicates that clustering femtocells using the JFCPA is more effective than random subchannel selection in terms of mitigating I^D_{FMu}.

The throughput gain is defined as the throughput of the femtocell tier divided by the corresponding throughput loss of the macrocell tier. As shown in Fig. 13, the throughput gain brought by the femtocell tier compensates well for the loss of the macrocell tier. For example, when $\Phi_C = 0$ and the number of femtocells is 200, the femtocell tier yields 22.5 dB throughput gain. In addition, the throughput loss of the macrocell tier can also be compensated for by the femtocell hybrid access mode, where fBSs open portions of their frequency bandwidth for non-CSG mMSs in the vicinity.

V. CONCLUSION

In this paper, we considered the design of a hybrid scheme for frequency resources allocation on the basis of the FMOS model with ISA and NISA, and the proposed JFCPA to achieve this hybrid scheme. In the JFCPA, three frequency bands are dynamically divided according to the density and the location of femtocells. The femtocells and the macrocell reuse the FMOS reuse band, which corresponds to the frequency reuse portion of the overall system bandwidth. The macrocell dedicated band is the macrocell-only portion, which solves the problem of dead-zones around femtocells and guarantees quality of service in the macrocell tier. The femtocell dedicated band is only available for the femtocell tier. Simulation results confirmed that the proposed hybrid scheme mitigates cross-tier and co-tier interference, improves spectrum efficiency, and yields higher throughput gain.

The difference between the single-macrocell scenario and the multi-macrocell scenario is that there is one more ISA in the macrocellular edge because of inter-cell interference, which can also be determined by SMA-based power control. Therefore, the JFCPA can also be applied in the multi-macrocell scenario. Our future work will study the distributed realization of the JFCPA, the optimal assignment strategy for the femtocell dedicated band, and combination methods for the JFCPA and soft frequency reuse [32] in the multi-macrocell scenario.

APPENDIX

A. Derivation of Clustering Threshold Distance R_{th}

We consider a simple femtocell environment comprising two femtocells as illustrated in Fig. 14. The target fBS i to its serving fMS $\hat{i}$ with transmit power $P^{\text{fBS}}_{\hat{i}}$ and interfering fBS j with transmit power $P^{\text{fBS}}_{\hat{j}}$ are located at $(0,0)$ and $(R,0)$, respectively. Neglecting the shadowing effects, the SIR of fMS $\hat{i}$,

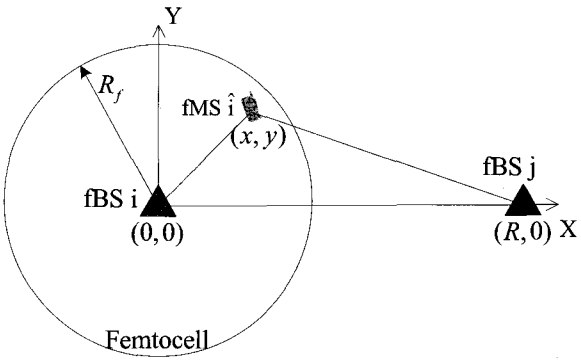

Fig. 14. Scenario for R_{th} derivation.

which is located at (x, y), can be calculated using

$$\mathrm{SIR} = \frac{P_{\hat{i}}^{\mathrm{fBS}} K_f (x^2+y^2)^{-\beta/2}}{P_{\hat{j}}^{\mathrm{fBS}} K_f [(R-x)^2+y^2]^{-\beta/2} WL^{-2}} = \Upsilon \tag{23}$$

where $(x^2+y^2)^{1/2}$ and $[(R-x)^2+y^2]^{1/2}$ are the distance from the fBS i and the distance from the fBS j to fMS $\hat{i}$, respectively; WL is the penetration loss; and Υ is the lowest target SIR of all fMSs. Assuming $P_{\hat{i}}^{\mathrm{fBS}} = P_{\hat{j}}^{\mathrm{fBS}}$ and rearranging (23) according to the definition of R_{th}, the following maximization problem can be obtained

$$\begin{aligned} \max \quad & R = \sqrt{(\Upsilon WL^{-2})^{\frac{2}{\beta}}(x^2+y^2) - y^2} + x \\ \text{s.t.} \quad & x^2 + y^2 \le R_f^2, \\ & -R_f \le x, y \le R_f. \end{aligned} \tag{24}$$

From (24), we can say that $\max\{x^2+y^2\} = R_f^2$, $\min\{y^2\} = 0$, and $\max\{x\} = R_f$ hold for all conditions. Therefore, R_{th} is calculated as

$$R_{th} = R_f[1 + (\Upsilon WL^{-2})^{\frac{1}{\beta}}]. \tag{25}$$

B. Proof and analysis of SMA 1)

According to the different causes of terms in (15), (15) can be divided into three parts

$$P_i = \underbrace{\Upsilon_i \sum_{j \in \mathbb{R}_l', j \neq i} P_j \frac{G_{ij}^{f2}}{G_{ii}^{f1}}}_{\text{(A) Interference between femtocells}} + \underbrace{\frac{\Upsilon_i}{G_{ii}^{f1}} N_0}_{\text{(B) Gaussian noise}} + \underbrace{\frac{\Upsilon_i G_{Mi}^{m2}}{G_{ii}^{f1}} P_{\mathrm{mBS}}}_{\text{(C) Interference from mBS}} \tag{26}$$

When femtocell i is close enough to the mBS, part (C) of (26) can be much greater than part (A), i.e., $P_{\mathrm{mBS}} G_{Mi}^{m2} \gg \sum_{j \in \mathbb{R}_l', j \neq i} P_j G_{ij}^{f2}$. Further, because $P_{\mathrm{mBS}} G_{M_i}^{m2} \gg N_0$, rearranging (26) leads to the following expression (omitting shadowing effects)

$$P_i \approx \frac{\Upsilon_i G_{M_i}^{m2}}{G_{ii}^{f1}} P_{\mathrm{mBS}}. \tag{27}$$

From the postulated condition, the power solution P_i is greater than the maximal power of each subchannel, i.e., $P_i > P_{\mathrm{fBS}}^{s-\max}$. Inserting this inequality into (27), we get

$$\frac{P_{\mathrm{fBS}}^{s-\max} G_{ii}^{f1}}{P_{\mathrm{mBS}} G_{Mi}^{m2}} < \Upsilon_i. \tag{28}$$

According to (28) and the definition of ISA, femtocell i should be located at ISA.

Hence, SMA 1) is proved.

C. Proof and Analysis of SMA 2)

$\mathbf{H}$ is undoubtedly a non-negative irreducible matrix. According to the Perron-Frobenious theorem [33], the spectral radius $\rho(\mathbf{H})$ is positive and satisfies the estimate

$$\min_i \sum_{j \neq i} \frac{G_{ij}^{f2}}{G_{ii}^{f1}} \Upsilon_i \le \rho(\mathbf{H}) \le \max_i \sum_{j \neq i} \frac{G_{ij}^{f2}}{G_{ii}^{f1}} \Upsilon_i. \tag{29}$$

According to theorem 3.9 in [34], if $\rho < 1$, then $(\mathbf{I} - \mathbf{H})$ is invertible and $(\mathbf{I} - \mathbf{H})^{-1}$ is positive. Thus, the power solution vector is positive, or $\mathbf{P} = (\mathbf{I} - \mathbf{H})^{-1}(\mathbf{N_0}\boldsymbol{\Upsilon} + \mathbf{P}_{\mathrm{mBS}}\hat{\boldsymbol{\Upsilon}}) > \mathbf{0}$. In light of the above analysis, if any $P_k \in (-P_{\mathrm{fBS}}^{s-\max}, 0)$ exists, removing the femtocell in accordance with (19) will make $\rho(\mathbf{H})$ tend toward the range $(0, 1)$, thus making $(\mathbf{I} - \mathbf{H})$ invertible and positive. Furthermore, if $(\mathbf{I} - \mathbf{H})^{-1}$ exists, the power solution is also proved to be the Pareto optimal solution in [26]. Hence, SMA 2) is proved.

REFERENCES

[1] V. Chandrasekhar, J. Andrews, and A. Gatherer, "Femtocell networks: A survey," *IEEE Commun. Mag.*, vol. 46, no. 9, pp. 59–67, Sept. 2008.
[2] 3GPP TS 22.220, "Service requirements for home node B (HNB) and home eNode B (HeNB)," v10.3.0.
[3] X. Lagrange, "Multitier cell design," *IEEE Commun. Mag.*, vol. 35, no. 8, pp. 60–64, Aug. 1997.
[4] 3GPP TR 25.967, "Home node B radio frequency (RF) requirements (FDD)," v9.0.0.
[5] Femto Forum, "Interference management in UMTS femtocells," [Online]. Available: http://www.femtoforum.org
[6] 3GPP TR 36.922, "LTE TDD home eNodeB RF requirements," v1.3.0.
[7] V. Chandrasekhar and J. G. Andrews, "Spectrum allocation in tiered cellular networks," *IEEE Trans. Commun.*, vol. 57, no. 10, pp. 3059–3068, Oct. 2009.
[8] H. Lee, D. Oh, and Y. Lee, "Mitigation of inter-femtocell interference with adaptive fractional frequency reuse," in *Proc. IEEE ICC*, Cape Town, South Africa, 2010, pp. 1–5.
[9] I. Guvenc, Moo-Ryong Jeong, and F. Watanabe, "A hybrid frequency assignment for femtocells and coverage area analysis for co-channel operation," *IEEE Commun. Letters*, vol. 12, no. 12, pp. 880–882, Dec. 2008.
[10] V. Chandrasekhar and J. G. Andrews, "Uplink capacity and interference avoidance for two-tier femtocell networks," *IEEE Trans. Wireless Commun.*, vol. 8, no. 7, pp. 3498–3509, July 2009.
[11] D. Lopez-Perez, G. de la Roche, A. Valcarce, A. Juttner, and J. Zhang, "Interference avoidance and dynamic frequency planning for WiMax femtocells networks," in *Proc. IEEE ICCS*, Singapore, Nov. 2008, pp. 1579–1584.
[12] H. Jo, C. Mun, J. Moon, and J. Yook, "Interference mitigation using uplink power control for two-tier femtocell networks," *IEEE Trans. Wireless Commun.*, vol. 8, pp. 4906–4910, Oct. 2009.
[13] X. Chu, Y. Wu, L. Benmesbah, and B. Ling, "Resource allocation in Hybrid macro/femto networks," in *Proc. IEEE WCNCW*, Sydney, Australia, Apr. 2010.
[14] 3GPP TR 36.814, "Further advancements for E-UTRA physical layer aspects," v9.0.0.
[15] DSL Forum TR-069. "CPE WAN Management Protocol."

[16] S. Kim, M. Yoo, and Y. Shin, "A weighted combining wireless location algorithm for mobile-WiMax femto-cell environment," *IEICE Trans. Commun.*, vol. E93-B, no. 3, Mar. 2010, pp. 749–752.
[17] 3GPP TR 36.300, "Evolved universal terrestrial radio access (E-UTRA) and evolved universal terrestrial radio access network (E-UTRAN)—overall description," v9.0.0.
[18] R4-092042, "Simulation assumption and parameters for FDD HeNB RF requirements," Alcatel-Lucent, PicoChip Designs, and Vodafone, 2009.
[19] IEEE, "Part 16: Air interface for fixed and mobile broadband wireless access systems," IEEE Std. 802.16e-2005, Feb. 2006.
[20] S. Sahni and T. Gonzalez, "P-complete approximation problems," *Journal of the ACM*, vol. 23, no. 3, pp. 555–565, July 1976.
[21] W. Fernandez, M. Karpinski, and C. Kenyon, "Approximation schemes for clustering problems," in *Proc. ACM STOC*, June 2003, pp. 50–58.
[22] R.Y. Chang, Z. Tao, J. Zhang, et al., "Multicell OFDMA downlink resource allocation using a graphic framework," *IEEE Trans. Veh. Technol.*, vol. 58, no. 7, pp. 3494–3507, Sept. 2009.
[23] A. Gibbons, *Algorithmic Graph Theory,* Melbourne, Sydney: Cambridge University Press, 1994.
[24] N. Bambos, and G.J. Pottie, "Power control based admission policies in cellular radio networks," in *Proc. IEEE GLOBECOM*, Orlando, USA, Dec. 1992, pp. 863–867.
[25] S.C. Chen, N. Bambos, and G.J. Pottie, "Admission control schemes for wireless communication networks with adjustable transmitter powers," in *Proc. IEEE INFOCOM*, Toronto, Canada, June 1994, pp. 21–28.
[26] N.D. Bambos, S.C. Chen, and G.J. Pottie, "Radio link admission algorithms for wireless networks with power control and active link quality protection," in *Proc. IEEE INFOCOM*, Boston, USA, Apr. 1995, pp. 97–104.
[27] N. Bambos, "Toward power-sensitive network architectures in wireless communications: Concepts issues, and design aspects," *IEEE Personal Commun.*, vol. 5, no. 3, pp. 50–59, June 1998.
[28] J. Zander, "Performance of optimum transmitter power control in cellular radio systems," *IEEE Trans. Veh. Technol.*, vol. 41, no. 1, pp. 57–62, Feb. 1992.
[29] J. G. Proakis, *Digital Communications,* McGraw-Hill Companies, Inc., 2004.
[30] D. S. Baum, J. Hansen, and J. Solo, "An interim channel model for beyond-3G system: Extending the 3GPP spatial channel model (SCM)," in *Proc. IEEE VTC*, Stockholm, Sweden, May 2005, pp. 3132–3136.
[31] B. Bollobas, *Modern Graph Theory,* New York: Springer-Verlag Inc., 1988.
[32] R1-050507, "Soft frequency reuse scheme for UTRAN LTE," Huawei, 3GPP TSG RAN Meeting 41, Athens, Greece, May 2005.
[33] F.R. Gantmacher, *The Theory of Matrices,* New York: Chelsea, 1974.
[34] R. S. Varga, *Matrix Iterative Analysis,* Englewood Cliffs, NJ: Prentice-Hall, 1962.

Hongjia Li received his B.S. degree in Information and Communication Engineering and M.S. degree in Control Theory and Control Engineering both from Qingdao University of Science and Technology in 2005 and 2008 separately. He received his Ph.D. degree of Circuit and System in Beijing University of Posts and Telecommunications (BUPT). In 2011, he joined the Institute of Acoustics, Chinese Academy of Sciences as an Assistant Professor. His research interests cover advanced mobile communication systems and the key technologies, including heterogeneous network (HetNet), radio resource management, green communications, and cognitive networks.

Xiaodong Xu received his B.S. degree in Information and Communication Engineering and M.S. degree in Communication and Information System both from Shandong University in 2001 and 2004 separately. He received his Ph.D. degrees of Circuit and System in Beijing University of Posts and Telecommunications (BUPT). His research interests cover advanced mobile communication systems and the key technologies, including generalized distributed network architecture, radio resource management, coordinated multi-point for next generation mobile system, and standardization of Enhanced 3G systems.

Dan Hu received her B.S. degree in Measurement and Control Technology and Instrumentation Program from Jilin University in 2009. She is currently a M.S. degree Candidate of Communication and Information System in Beijing University of Posts and Telecommunications (BUPT). Her research interests cover advanced mobile communication systems and the key technologies, including standardization of 3GPP LTE/LTE-A, and heterogeneous network (HetNet).

Xiaofeng Tao received his B.S. degree in Electrical Engineering from Xi'an Jiaotong University, China, in 1993, and M.S.E.E. and Ph.D. degrees in Telecommunication Engineering from Beijing University of Posts and Telecommunications in 1999 and 2002, respectively. He was a Research Engineer Working in the Posts and Telecommunications Industry Company of China (PTIC) from 1993 to 1996. He is currently the Professor and Vice Director of WTI of BUPT and a Group Leader of the TDD Special Working Group of China 863 FuTURE Program. His research interests cover techniques for B3G, such as space-time coding, MIMO, novel cell structures, and intelligent group handover mode.

Ping Zhang received the M.S. degree from Northwestern Polytechnical University, Xi'an, China, in 1986 and the Ph.D. degree from Beijing University of Posts and Telecommunications, Beijing, China, in 1990, both in electronics engineering. From 1994 to 1995, he was a Post-Doctoral Researcher in the PCS Department, Korea Telecom Wireless System Development Center. Now, he is the Professor of BUPT, Director of Wireless Technology Innovation Labs, Member of the China 3G and B3G group, Senior Consultant of NTT DoCoMo, and Member of WWRF Vision Committee. His research interests cover the key techniques of the beyond 3G and 3G systems, especially in the multiple access technique, modulation, and channel coding.

Song Ci is an Assistant Professor of Computer and Electronics Engineering at the University of Nebraska-Lincoln. He is the Director of the Intelligent Ubiquitous Computing Lab (iUbiComp Lab) and holds a courtesy appointment of UNL Ph.D. in the Biomedical Engineering Program. He is also affiliated with Nebraska Biomechanics Core Facility at the University of Nebraska at Omaha and Center for Advanced Surgical Technology (CAST) at University of Nebraska Medical Center, Omaha, NE. His research interests include dynamic complex system modeling and optimization, green computing and power management, content-aware quality-driven cross-layer optimized multimedia over wireless, cognitive network management and service-oriented architecture, and cyber-enable e-health care.

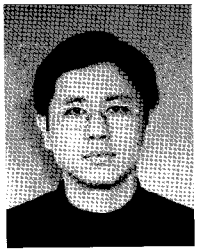

Hui Tang received the B.S. degree from Lanzhou University in 1992, the M.S. degree from the Institute of Computing Technology of the Chinese Academy of Sciences in 1995, and the Ph.D. degree from the Institute of Acoustics of the Chinese Academy of Sciences in 1998. Since 2004, he has become the Founding Director of the High Performance Network Laboratory of the Institute of Acoustics of the Chinese Academy of Sciences, and his team has undertaken several key national projects. Since 2008, he has served on the Executive Committee of the National Key Project "The Next Generation Broadband Wireless Mobile Network." His research interests include next generation Internet, wireless multimedia technologies, Internet of things, mobile Internet, and p2p technologies.